SYNTHESIS, CRYSTAL STRUCTURES AND MAGNETIC PROPERTIES OF COORDINATION COMPOUNDS WITH NITRONYL NITROXIDE RADICALS AND [M(HFAC)₂] (M = CUᴵᴵ AND MNᴵᴵ)

Yan-Li Gao[a,*,iD], Yufei Wang[a], Huijin Liu[a], Xiaoli Song[a], Yali Wang[a], Ting Su[a] and Shiqing Bi[a]

[a]School of Chemistry and Chemical Engineering, Yulin University, Yulin 719000, P. R. of China

The reaction of metal hexafluoroacetylacetonato [Mᴵᴵ(hfac)₂, M = Cu, Mn] with the stable nitronyl nitroxide 2–(3–isobutyl–pyrazole)–4,4,5,5–tetramethylimidazoline–1–oxyl–3–oxide (L), resulted in one dimensional zig–zag chain systems [{Cu(hfac)₂}₂L₂]ₙ and [CuMn(hfac)₄L₂]ₙ. The main feature inherent in the nature of [{Cu(hfac)₂}₂L₂]ₙ single crystals is their ability to undergo reversible structural rearrangements with temperature variation, accompanied by anomalies of magnetism. The value of χₘT shown strongly antiferromagnetic at low temperature and becomes ferromagnetic when the temperature increases. And the heteronuclear complex [CuMn(hfac)₄L₂]ₙ shows antiferromagnetic interactions between manganese and nitronyl nitroxide.

Keywords: nitronyl nitroxide; Mᴵᴵ(hfac)₂ complexes; X–ray crystal structure; spin–crossover–like; magnetic property.

INTRODUCTION

The study of metal–organic radical complexes has attracted more and more attention in the past few decades due to the intriguing magnetic interactions between metal ions and the organic spin carriers.[1–3] Among the commonly used organic radicals, nitronyl nitroxide radicals (NITR) are more particularly attractive because they are stable, easy to synthesize and favor the onset of bulk magnetic properties in the solid–state. Their metal complexes are characterized by strong exchange couplings between organic and metal unpaired electrons, and properties highly dependent on the structure of the free radical and the nature of the metal ion.[4–9] In addition, modifying the substituted R groups of NITR with functional coordination groups can generate various metal-radical complexes with various magnetic properties.[10–17]

The development of methods for synthesizing Cu(II) complexes with nitroxides underlies the creation of unusual heterospin compounds, which exhibit thermo– and photoinduced spin transitions.[18–20] A spin–crossover–like phenomenon is observed when the external effect changes the mutual orientation of the paramagnetic centers and consequently the character of interaction of unpaired electrons.[21–25] The thermally induced change in the distances between the paramagnetic centers in the {>N–˙O–Cuᴵᴵ} or {>N–˙O–Cuᴵᴵ–O˙–N<} exchange clusters generally leads to an abrupt change in the energy and, or sign of the exchange interaction, which gives rise to an anomaly on the curve in the temperature dependence of the effective magnetic moment (μₑff). They are often called "breathing crystals" because of the large–scale changes of the unit cell volume upon transition.[26-28] In addition, the indication can be optical because the compound changes color during the transition.

Herein, we synthesized the nitronyl nitroxide ligands 2–(4–isobutyl–pyrazole)–4,4,5,5–tetramethylimidazoline–1–oxyl–3–oxide (L), and then were reacted with metal hexafluoroacetylacetonato [Mᴵᴵ(hfac)₂, M = Cu, Mn]. The gradual magnetostructural transition in breathing crystals based on copper(II) and heteronuclear complex based on copper(II) and manganese(II) were successfully synthesized. Further analyses of the structures and magnetism of the metal–radical compounds were reported.

*e-mail: gaoyanli8503@126.com

EXPERIMENTAL

Materials and methods

All reagents were obtained from commercial sources and used without further purification. The nitroxide radical L was prepared as reported previously.[29-31]

Preparation of [{Cu(hfac)₂}₂L₂]ₙ

Cuᴵᴵ(hfac)₂(H₂O)₂ (1 mmol, 51.4 mg) was dissolved in hot *n*-heptane 10 mL, and then the solution was cooled to about 50 °C. L (0.05 mmol, 15 mg), dissolved in 2 mL of CHCl₃, was added with constant stirring. The solution was stirred for *ca*. 3 minutes and then cooled to room temperature. The filtrate was kept under an N₂ stream at room temperature until a solid appeared. A few drops of CHCl₃ were added in the flask until the solid disappeared, sealed and placed in a refrigerator. After 2–3 d, 54.5 mg block–shaped dark-blue crystals were obtained (yield 82%). Anal Calcd for C₄₈H₅₀Cu₂N₈O₁₂ are: C, 38.04, H, 3.30, N, 7.40. Found : C, 38.23, H, 3.17, N, 7.51. FTIR (KBr, cm⁻¹): 1661(s), 1557(w), 1533(s), 1476(s), 1358(w), 1 223(s), 1145(s), 1084(s), 861(s), 798(w), 665(s), 614(s).

Preparation of [CuMn(hfac)₄L₂]ₙ

The method for the synthesis was similar to used for preparadion of [Cu(hfac)₂L]ₙ except that Mn(hfac)₂ and Cu(hfac)₂ (The molar ratio is 1:1). 54.1 mg dark–blue crystals were obtained (yield 86%). Anal Calcd for C₄₈H₅₀CuMnN₈O₁₂ are: C, 38.52, H, 3.37, N, 7.49. Found (%): C, 38.21, H, 3.22, N, 7.41. FTIR (KBr, cm⁻¹): 1619(s), 1562(s), 1536(s), 1499(s), 1250(s), 1212(s), 801(s), 767(w), 747(w), 667(s), 591(s).

General characterizations

Infrared spectra were recorded on a JASCO FT/IR–660 PLUS spectrometer by transmission through KBr pellets in the range of 400–4000 cm⁻¹. Elemental analyses for C, H, and N was carried out using a PerkinElmer series II CHNS/O Analyzer 2400. The magnetization measurements on the crystalline solids were carried out using Quantum Design MPMS–5S and MPMS–2 SQUID magnetometers. The magnetic field were varied from −50 to 50 kOe and the temperature from 2–300 K. The data are corrected for sample diamagnetism using Pascal's constants.[32,33]

Single crystal x−ray diffraction studies

X−ray diffraction intensities were collected for the selected single crystals individually mounted on glass fibers at room temperature using Bruker diffractometers: SMART−APEX II with a CCD and D8−QUEST with a CMOS area detector. Both employed graphite-monochromated MoKα (λ = 0.71073 Å) radiation. Data reduction was made using SAINT and the intensities were corrected for absorption by SADABS.[34-35] The structures were solved by direct methods and refined by full-matrix least-squares against F^2 using ShelXL.[36] Part of the hydrogen atoms were located in the difference Fourier maps and those not found were added at theoretical positions using the riding model. CCDC contains the supplementary crystallographic data for this paper (2089053 for 296 K, 2089054 for 100 K of copper complex and 2089055 for 173 K of manganese-copper complex). The details can be obtained from the cif files deposited at the Cambridge Crystallographic Data Centre via www.ccdc.cam.ac.uk/structures.

RESULTS AND DISCUSSION

Structure descriptions

Dark−blue crystals of the $[\{Cu(hfac)_2\}_2L_2]_n$ and $[CuMn(hfac)_4L_2]_n$ heterospin complex are readily isolated with a high yield from the hexane solution of the equimolar amounts of $M(hfac)_2$ and L. The synthesis of the complex is reproducible, and there are no impurities in the product. The molecular structures of $[\{Cu(hfac)_2\}_2L_2]_n$ and $[CuMn(hfac)_4L_2]_n$ were successfully determined using X−ray crystallographic analysis at different temperature. The crystal and refinement data are summarized in Table 1. Complexes

Table 1. Crystallographic data and refinement parameters for two complexes at different temperatures

	$[\{Cu(hfac)_2\}_2L_2]_n$		$[CuMn(hfac)_4L_2]_n$
Temp.	296(2) K	100(2) K	173(2) K
formula	$C_{48}H_{50}Cu_2F_{24}N_8O_{12}$	$C_{48}H_{50}Cu_2F_{24}N_8O_{12}$	$C_{48}H_{50}MnCuF_{24}N_8O_{12}$
fw	1514.04	1514.04	1505.44
cryst syst	monoclinic	monoclinic	monoclinic
Space group	*C* 2/*c*	*C* 2/*c*	*C* 2/*c*
a (Å)	31.3211(15)	30.7255(15)	30.8643(15)
b (Å)	9.6832(4)	9.5752(4)	9.6009(4)
c (Å)	26.214(2)	25.0581(12)	25.9176(19)
β (°)	125.6390(10)	123.9180(10)	125.1944(11)
V (Å³)	6461.3(6)	6117.7(5)	6276.1(6)
D_c / (g·cm⁻³)	1.556	1.644	1.593
Z	4	4	4
Refls. Total	81337	55327	61143
Unique	9786	9436	9872
Param.	433	442	503
R_{int}	0.0225	0.0172	0.0314
R_1/wR_2 *[I>2σ(I)]*	0.0749 0.2234	0.0591 0.1550	0.0814 0.2401
R_1/wR_2 (all data)	0.0971 0.2501	0.0661 0.1619	0.0941 0.2542
GoF	1.047	1.034	1.049
Complet.	0.996	0.984	0.995
Theta (°)	28.42	28.36	28.34

$[\{Cu(hfac)_2\}_2L_2]_n$ and $[CuMn(hfac)_4L_2]_n$ crystallize in the monoclinic space group *C2/c* with Z = 4. Selected bond lengths and angles are listed in Tables 2 and 3, respectively.

Table 2. Selected bond lengths [Å] for complexes $[\{Cu(hfac)_2\}_2L_2]_n$ and $[CuMn(hfac)_4L_2]_n$

$[\{Cu(hfac)_2\}_2L_2]_n$				$[CuMn(hfac)_4L_2]_n$	
296 K/[Å]		100 K/[Å]		173 K/[Å]	
N1-O1	1.299(4)	N1-O1	1.309(3)	N1-O1	1.305(4)
N2-O2	1.271(5)	N2-O2	1.276(3)	N2-O2	1.275(5)
Cu1-O1	2.230(3)	Cu1-O1	2.001(2)	Mn1-O1	2.147(3)
Cu1-O3	2.061(4)	Cu1-O3	2.319(2)	Mn1-O3	2.158(3)
Cu1-O4	1.966(3)	Cu1-O4	1.958(2)	Mn1-O4	2.131(3)
Cu2-N3	2.492(3)	Cu2-N3	2.457(3)	Cu1-N3	2.438(3)
Cu2-O5	1.955(3)	Cu2-O5	1.975(2)	Cu1-O5	1.995(3)
Cu2-O6	1.964(3)	Cu2-O6	1.953(2)	Cu1-O6	1.981(3)

Figure 1 shows the asymmetric unit and a polymer chain of complex $[\{Cu(hfac)_2\}_2L_2]_n$. The molecular structure consists of the alternate copper-radical zig−zag chain running parallel to one another; that radical plays a crucial role in establishing this one-dimensional character, since it acts as a bidentate ligand, connecting metal ions. In the chain complexes, the CuO_4 square environment in the $Cu(hfac)_2$ coordination matrices is a distorted octahedron. The metal ion Cu1 is six coordinated by two oxygen atoms of the nitronyl nitroxide fragments, which is lying in the $Cu1N_2O_4$ coordination units alternate with the {>N1−ˈO1−Cuᴵᴵ−ˈO1−N1<} heterospin clusters based on the "head−to−head" motif. The second oxygen atom of the nitronyl nitroxide fragment N2−O2 is not involved in coordination. The structural dynamics in the chains due to temperature variation are mainly related to the rearrangement of the $Cu1O_6$ coordination units. The Cu2 ion is also coordinated by two nitrogen atoms of the pyrazole rings of the two bridgings bidentate L. Thus, the N3 atom occupied axial coordination sites. As a result, the apical Cu2−N3 bond length is 2.493 Å, while the equatorial Cu2−O(hfac) are much shorter than the apical bonds (around 1.958 Å).

With the decrease in the temperature, the Cu1−O1 and Cu1-O3 bond lengths in the $Cu1O_6$ units are drastically changed which was shown in Figure 2. At high temperatures (*T*~296 K), coordination octahedra $Cu1O_6$ are elongated along the direction of the O1−Cu1−O1 axis, in which the Cu1−O1 distance is 2.229 Å. The Cu1−O1 bond shorted from 2.229 to 2.001 Å when the crystal is cooled from 296 K to 100 K, accompanied by a simultaneous lengthening of two Cu1−O3 bonds from 2.061 to 2.319 Å in one of the directions. With the decrease of temperature, the direction the elongated Jahn−Teller axis changed in the $Cu1O_6$ units. At high temperatures, the axis is O1−Cu1−O1, while at low temperatures, the axis changed to O3−Cu1−O3. As a result, on lowering the temperature from 296 to 100 K, the nitroxides pass from axial to equatorial coordination positions of copper(II) ion. This rearrangement is accompanied by a switch of exchange interaction in spin triads nitroxide−copper(II)−nitroxide from weak ferromagnetic to a strong antiferromagnetic one.

For compound $[CuMn(hfac)_4L_2]_n$, the ligand L coordinated through the oxygen atom of the NOˈ and N atom of pyrazole linkage to the metal leading to a zig−zag chain, as depicted in Figure 3. The asymmetric unit of complex consists of two half of metal atoms. One with a nearly octahedral coordination (Mn) which are occupied by four oxygen atoms (O3, O4) from two hfac units, two oxygen atoms (O1) from two nitroxide ligands. The other is elongated octahedron geometry (Cu) with hfac oxygen atoms (O5, O6) at the base and two pyrazole

Table 3. Selected angles [°] for complexes $[\{Cu(hfac)_2\}_2L_2]_n$ and $[CuMn(hfac)_4L_2]_n$

	$[\{Cu(hfac)_2\}_2L_2]_n$			$[CuMn(hfac)_4L_2]_n$	
296 K/[°]		100 K/[°]		173 K/[°]	
N1-O1-Cu1	127.7(2)	N1-O1-Cu1	127.7(2)	N1-O1-Mn1	128.9(2)
O1-Cu1-O3	98.84(11)	O1-Cu1-O3	100.76(8)	O1-Mn1-O3	98.01(10)
O1-Cu1-O4	92.91(11)	O1-Cu1-O4	92.21(8)	O1-Mn1-O4	92.83(10)
O3-Cu1-O4	91.08(13)	O3-Cu1-O4	95.17(8)	O3-Mn1-O4	96.33(11)
O5-Cu2-N3	96.02(12)	O5-Cu2-N3	90.26(9)	O5-Cu1-N3	90.18(11)
O6-Cu2-N3	90.30(12)	O6-Cu2-N3	96.35(9)	O6-Cu1-N3	96.16(12)
O5-Cu2-O6	92.21(12)	O5-Cu2-O6	92.74(9)	O5-Cu1-O6	91.17(12)
N4-N3-Cu2	132.4(2)	N4-N3-Cu2	131.3(4)	N4-N3-Cu1	131.8(3)
C4-N3-Cu2	123.0(3)	C4-N3-Cu2	123.0(2)	C4-N3-Cu1	123.0(3)
C23-O3-Cu1	125.0(3)	C23-O3-Cu1	121.4(2)	C23-O3-Mn1	127.6(3)
C21-O4-Cu1	126.1(3)	C21-O4-Cu1	129.6(2)	C21-O4-Mn1	127.7(3)
C16-O6-Cu2	124.1(3)	C16-O6-Cu2	124.3(2)	C16-O6-Cu1	124.6(3)
C18-O5-Cu2	124.0(3)	C18-O5-Cu2	123.8(2)	C18-O5-Cu1	124.8(3)
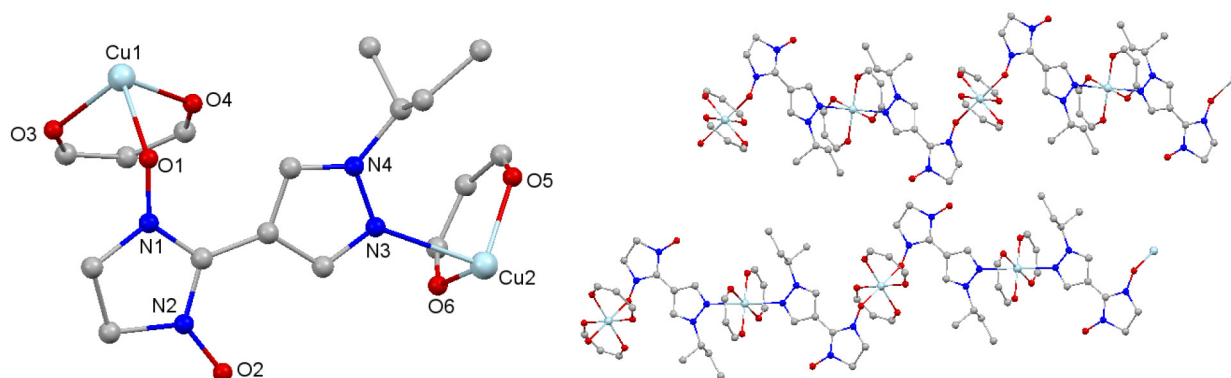
Figure 1. *The structural of asymmetric unit (left) and the fragment of chain (right) of compound $[\{Cu(hfac)_2\}_2L_2]_n$. Fluorine, hydrogen and part carbon atoms are omitted for clarity*
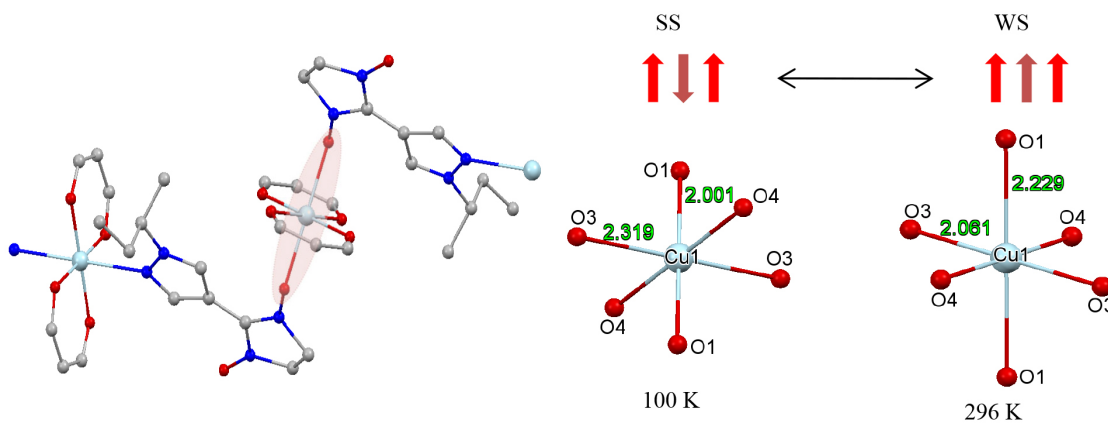
Figure 2. *Copper(1) environments at 296 K and 100 K*

nitrogen atoms (N3) at the apex. The Mn1−O1 bond length is 2.146 Å, while the Mn1−O(hfac) is close to the bond (2.131 Å and 2.158 Å), and the Cu1−N3 bond length is 2.438 Å while the Cu1−O(hfac) are much shorter (1.981 Å and 1.995 Å). The angle of N1−O1−Mn1 is 128.89°. The nearest intrachain metal−metal distances are provided by Mn···Cu distance of 8.081 Å while the interchain Mn···Cu distance of 10.861 Å. In addition, there are two somewhat longer intermolecular F···F interaction (3.105 Å and 3.066 Å) which bridges the chains into layers. And one slightly longer intermolecular F···C interaction (3.110 Å) bridges the chains into network as shown in Figure 4.

Magnetic properties

The temperature-dependent magnetic susceptibilities of the complex were measured in the temperature range 2−300 K in an external magnetic field of 5 kOe. The data were corrected for the diamagnetism of the components.

The temperature dependence of $\chi_m T$ for complex $[\{Cu(hfac)_2\}_2L_2]_n$ was shown in Figure 5. The value of $\chi_m T$ was equal to 1.45 cm^3 K mol^{-1} at room temperature. In agreement with this structural data, the value of the effective magnetic moment of $[\{Cu(hfac)_2\}_2L_2]_n$ corresponds
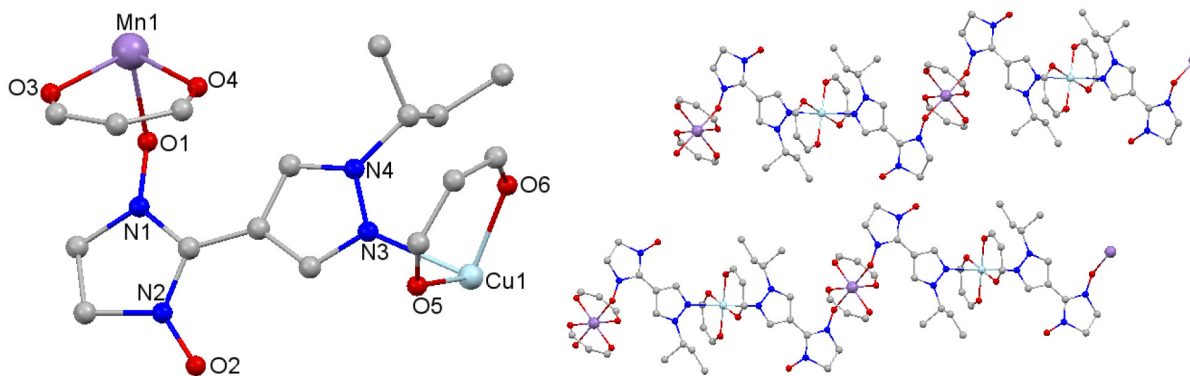
Figure 3. *The structural of asymmetric unit (left) and the fragment of chain (right) of compound [MnCu(hfac)₄L₂]ₙ. Fluorine and hydrogen atoms are omitted for clarity*
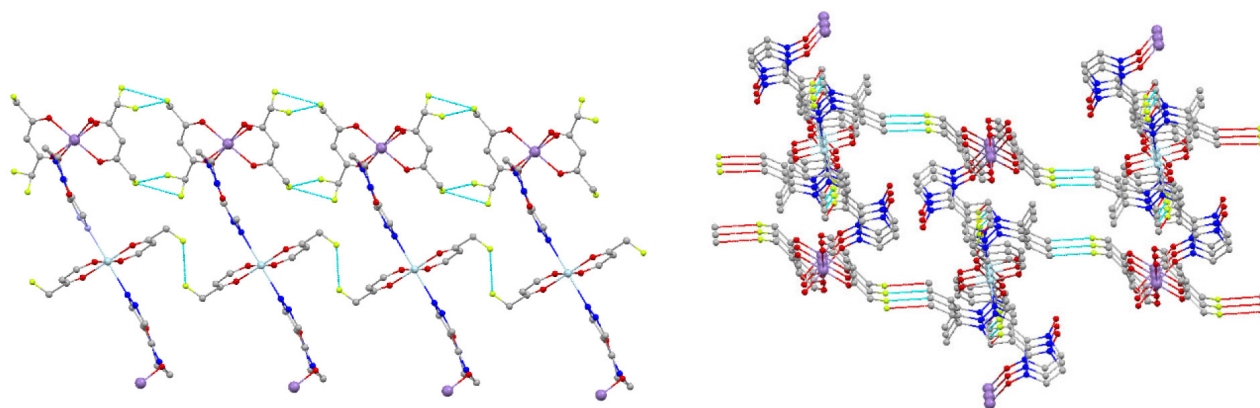
Figure 4. *Details of the crystal packing of complex [MnCu(hfac)₄L₂]ₙ of the F•••F (left) and F•••C (right) interchain short contacts are shown in green. Hydrogen and some fluorine and carbon atoms are omitted for clarity*
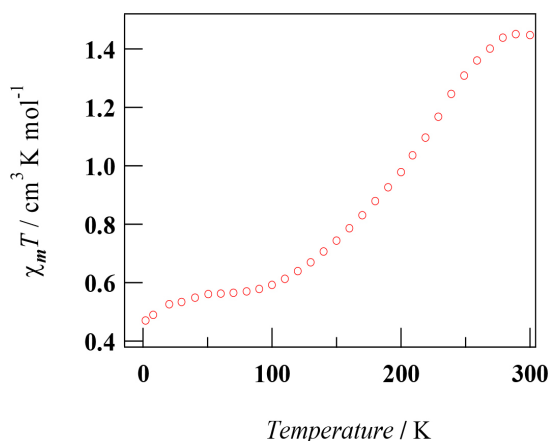
Figure 5. *Temperature dependence of $\chi_m T$ for complex [{Cu(hfac)₂}₂L₂]ₙ*

to the situation of two radicals and two Cu^{II} (2*0.375 + 2*0.4 = 1.55 cm³ mol⁻¹ K). The $\chi_m T$ value decreased sharply in the range 300–100 K. The magnetic moment becomes 0.6 cm³ K mol⁻¹ at 100 K, which corresponds to its decrease by a factor of 2 in the total number of spins. As the temperature is decreased, the Cu1–O1 distances is shorter, one Cu and one radical contributions are expected to be cancelled out due to strong antiferromagnetic Cu-·ON interactions. Following from this, a powerful antiferromagnetic exchange interaction dominates at low temperature, then the $\chi_m T$ value should be close to 0.75 cm³ mol⁻¹ K. It is responsible for the vanishing contribution to magnetic susceptibility from half of the total number of spins. As follows from the value of $\chi_m T$, the spin state conversion is essentially finished at $T < 100$ K. In the $Cu2N_2O_4$ units, the Cu2–N3 distances are shortened at

reduced temperatures but to a smaller extent than the Cu1–O1 distances.

Plots of the temperature dependence of the molar paramagnetic susceptibility and the effective magnetic moment for $[CuMn(hfac)_4L_2]_n$, are shown in Figure 6. At 300 K, $\chi_m T$ is equal to 3.67 cm³ K mol⁻¹, a value much lower than expected for non–interaction one $S_{Mn} = 5/2$, two $S_{rad} = 1/2$ spins and one $S_{Cu} = 1/2$ (They are 4.375, 0.75 and 0.375 cm³ K mol⁻¹ as g = 2, respectively). The gradual decrease of the $\chi_m T$ values at room temperatures indicates strong antiferromagnetic interactions between manganese(II) and nitroxide. As the temperature is lowered to 6 K, $\chi_m T$ gradually decreases to reach a plateau value of 3.00 cm³ K mol⁻¹. Below 6 K, the decrease of the $\chi_m T$ value can be attributed to weak intermolecular antiferromagnetic interactions. The susceptibility was fitted by the Curie-Weiss law leading to Curie and Weiss constants of C = 3.05 cm³ K mol⁻¹ and $\theta = -0.11$ K (the solid blue line). The observed susceptibility data for complex $[CuMn(hfac)_4L_2]_n$ were reproduced by a simplified model: three–spin (1/2−5/2−1/2) system plus one single Cu^{II} ion [$\hat{H} = -J (S_{Mn} \bullet S_{Rad1} + S_{Mn} \bullet S_{Rad2}) + S_{Cu}$] and a mean–field approximation to account for the weak magnetic interactions between Mn and radical. The best–fit achieved with g = 2.04, J = -134.7 cm⁻¹, and J' = -0.04 cm⁻¹ (the solid red line).

Complex $[\{Cu(hfac)_2\}_2L_2]_n$ reaches an almost saturated value of 1.82 Bohr magnetons at a magnetic field of 5 T at 2 K, being close to theory expected (2 $N\mu_B$). The behaves should correspond to two contribution, one resulting from antiferromagnetic interaction of Rad−Cu^{II}−Rad unit (S = 1/2) and one uncoupled Cu^{II} ion (S = 1/2). The magnetic data of 3.86 Bohr magnetons for the complex $[CuMn(hfac)_4L_2]_n$ shows that it behaves as expected for a S = 3/2 Rad–Mn^{II}–Rad antiferromagnetic triad and one Cu^{II} ion, being close to theory expected (Figure 7).
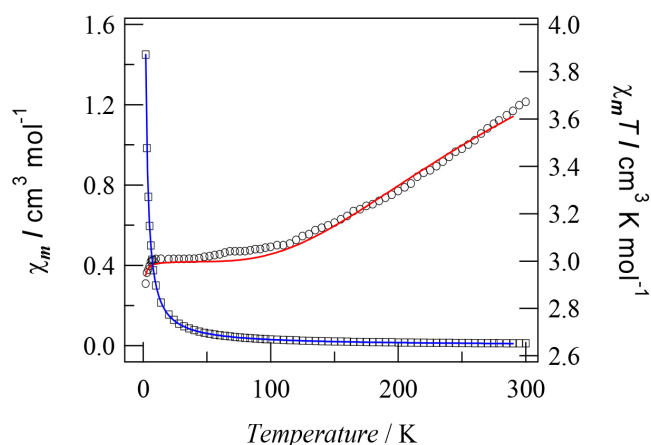
Figure 6. *Temperature dependence of χ$_m$ (square) and χ$_m$T (circular) for complex [CuMn(hfac)$_4$L$_2$]$_n$*
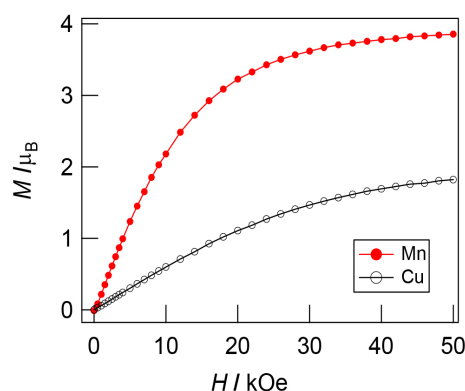
Figure 7. *Isothermal magnetization at 2 K of [{Cu(hfac)$_2$}$_2$L$_2$]$_n$ and [CuMn(hfac)$_4$L$_2$]$_n$*

CONCLUSIONS

One-dimensional chain complexes [{Cu(hfac)$_2$}$_2$L$_2$]$_n$ and [CuMn(hfac)$_4$L$_2$]$_n$ based on metal(II) and nitronyl nitroxide radicals have been successfully prepared. The single-crystal structures show that both compounds exhibit a one-dimensional chain structure in which Cu or/and Mn ions are linked by the oxygen atoms of NO$^•$ groups and the N atoms of the pyrazole rings. The complex [{Cu(hfac)$_2$}$_2$L$_2$]$_n$ studies revealed a spin-crossover-like phenomenon. The magnetic was changed from ferromagnetic interactions to antiferromagnetic interactions when the temperature decreased from 300 K to 100 K. The magnetic studies showed antiferromagnetic interactions for [CuMn(hfac)$_4$L$_2$]$_n$ compound, and the magnetic data were fitted using simplified models through Mn-radical plus one single Cu ion. Their magneto-structural correlations have been explained based on the crystal structures.

SUPPLEMENTARY MATERIAL

The checkCIF reports are available free of charge at http://quimicanova.sbq.org.br, in pdf format.

ACKNOWLEDGEMENTS

REFERENCES

1. Thorarinsdottir, A. E.; Harris, T. D.; *Chem. Rev.* **2020**, *120*, 8716. [Crossref]
2. Demir, S.; Jeon, I. R.; Long, J. R.; Harris, T. D.; *Coord. Chem. Rev.* **2015**, *289-290*, 149. [Crossref]
3. Ratera, I.; Veciana, J.; *Chem. Soc. Rev.* **2012**, *41*, 303. [Crossref]
4. Brook, D. J. R.; *Comments Inorg. Chem.* **2015**, *35*, 1. [Crossref]
5. Preuss, K. E.; *Coord, Chem. Rev.* **2015**, *289-290*, 49. [Crossref]
6. Li, H. D.; Jing, P.; Lu, J.; Xie, J.; Zhai, L. J.; Xi, L.; *Inorg. Chem.* **2021**, *60*, 7622. [Crossref]
7. Gao, Y.-L.; Nishihara, S.; Suzuki, T,; Umeo, K.; Inoue, K.; Kurmoo, M.; *Dalton Trans.* **2022**, *51*, 6682. [Crossref]
8. Fortier, S.; Le, R. J. J.; Chen, C. H.; Vieru, V.; Murugesu, M.; Chibotaru, L. F.; Mindiola, D. J.; Caulton, K. G.; *J. Am. Chem. Soc.* **2013**, *135*, 14670. [Crossref]
9. Huang, X. H,; Wang, K,; Han, J.; Xie, J. F.; Li, L. C.; Sutter, J-P.; *Dalton Trans.* **2021**, *50*, 11992. [Crossref]
10. Witt, A.; Heinemann, F. W.; Khusniyarov, M. M.; *Chem. Sci.* **2015**, *6*, 4599. [Crossref]
11. Han, J.; Xi, L.; Huang, X. H.; Li, L. C.; *Cryst. Growth Des.* **2021**, 21, 7186. [Crossref]
12. Evgeny, V. T.; Pavl, V. P.; Svetlana, I. Z.; Dmitry, E. G.; Nina, P. G.; Matvey, V. F.; Dmitri, V. S.; Rimma, I. S.; Irina, Y. B.; Inna, K. S.; Artem, S. B.; Maxim, S. K.; Pavel, S. P.; Marina, E. T.; Ovcharenko, V. I.; *J. Am. Chem. So*c. **2021**, *143*, 8164. [Crossref]
13. Tanimoto, R.; Wada, T.; Okada, K.; Shiomi, D.; Sato, K.; Takui, T.; Suzuki, S.; Naota, T.; Kozaki, M.; *Inorg. Chem.* **2022**, *61*, 3018. [Crossref]
14. Wang, J.; Li, J. N.; Zhang, S. L.; Zhao, X. H.; Shao, D.; Wang, X. Y.; *Chem. Comm.* **2016**, *52*, 5033. [Crossref]
15. Gao, Y.-L.; Wang, Y. F.; Gao, L. G.; Li, J.; Wang, Y. L.; Inoue, K.; *ACS Omega* **2022**, *7*, 10022. [Crossref]
16. Rausch, R.; Krause, A. M.; Krummenacher, I.; Braunschweig, H.; Würthner, F.; *J. Org. Chem.* **2021**, *86*, 2447. [Crossref]
17. Xi, L.; Li H. D.; Sun J.; Ma Y.; Tang J. K.; Li L. C.; *Inorg. Chem.* **2020**, *59*, 443. [Crossref]
18. Lanfranc de, P. F.; Belorizky, E.; Calemczuk, R.; Luneau, D.; Marcenat, C.; Ressouche, E.; Turek, P.; Rey, P.; *J. Am. Chem. Soc.* **1995**, *117*, 11247. [Crossref]
19. Rey, P.; Ovcharenko, V. I.; *In Magnetism: Molecules to Materials*; IV; Miller, J. S.; Drillon, M.; eds.; Wiley-VCH: New York, 2003, p 41.
20. Fedin, M.; Ovcharenko, V.; Sagdeev, R.; Reijerse, E.; Lubitz, W.; Bagryanskaya, E.; *Angew. Chem., Int. Ed.* **2008**; *47*, 6897. [Crossref]
21. Ovcharenko, V. I.; Romanenko, G. V.; Maryunina, K. Y.; Bogomyakov, A. S.; Gorelik, E. V.; *Inorg. Chem.* **2008**, *47*, 9537. [Crossref]
22. Romanenko, G. V.; Maryunina, K. Y.; Bogomyakov, A. S.; Sagdeev, R. Z.; Ovcharenko, V. I.; *Inorg. Chem.* **2011**, *50*, 6597. [Crossref]
23. Ovcharenko, V. I.; Bagryanskaya, E. G.; *In Spin-Crossover Materials: Properties and Applications*; Halcrow, M. A., ed.; 1st ed., John Wiley & Sons, Ltd.: New York, 2013, pp 239.
24. Fedin, M. V.; Veber, S. L.; Bagryanskaya, E. G.; Ovcharenko, V. I.; *Coord. Chem. Rev.* **2015**, *289-290*, 341. [Crossref]
25. Okazawa, A.; Hashizume, D.; Ishida, T.; *J. Am. Chem. Soc.* **2010**, *132*, 11516. [Crossref]
26. Tretyakov, E. V.; Tolstikov, S. E.; Suvorova, A. O.; Polushkin, A. V.; Romanenko, G. V.; Bogomyakov, A. S.; Veber, S. L.; Fedin, M. V.; Stass,

D. V.; Reijerse, E.; Lubitz, W.; Zueva, E. M.; Ovcharenko, V. I.; *Inorg. Chem.* **2012**, *51*, 9385. [Crossref]

27. Tretyakov, E. V.; Romanenko, G. V.; Veber, S. L.; Fedin, M. V.; Polushkin, A. V.; Tkacheva, A. O.; Ovcharenko, V. I.; *Aust. J. Chem.* **2015**, *68*, 970. [Crossref]

28. Kaszub, W.; Marino, A.; Lorenc, M.; Collet, E.; Bagryanskaya, E. G.; Tretyakov, E. V.; Ovcharenko, V. I.; Fedin, M. V.; *Angew. Chem., Int. Ed.* **2014**, *53*, 10636. [Crossref]

29. Ullman, F. E.; Osiecki, J. H.; Boocock, D. G. B.; Darcy R.; *J. Am. Chem. Soc.* **1972**, *94*, 7049. [Crossref]

30. Hirel, C.; Vostrikova, K. E.; Pécaut, J.; Ovcharenko, V. I.; Rey, P.; *Chem. Eur. J.* **2001**, *7*, 2007. [Crossref]

31. Victor, O.; Sergey, F.; Elvina, C.; Galina, R.; Artem, B.; Zhanna, D.; Nikita, L.; Vitaly, M.; Marina, P.; Maria, P.; Ekaterina, Z.; Igor, R.; Elena, R.; Galina, L.; Renad, S.; *Inorg. Chem.* **2016**, *55*, 5853. [Crossref]

32. Boudreaux, E. A.; Mulay, L. N.; *Theory and Application of Molecular Paramagnetism*; John Wiley & Sons: New York, 1976, p491.

33. Gordon, A. B.; John, F. B.; *J. Chem. Educ.* **2008**, *85*, 532. [Crossref]

34. SAINT-Plus. Bruker Analytical X-ray System, version 6.02; Madison; Wiley: 1999.

35. Sheldrick, G. M.; SADABS — *An Empirical Absorption Correction Program*; Wiley, Bruker Analytical X-ray Systems, Madison, 1996.

36. Sheldrick, G. M.; *Acta Crystallogr., Sect. C: Struct. Chem.* **2015**, *71*, 3. [Crossref]